Structure and activity of oxidized Pt(110) and α-PtO_2

Thorbjørn M. Pedersen,[a] Wei Xue Li[ab] and Bjørk Hammer*[a]

Received 26th October 2005, Accepted 1st February 2006
First published as an Advance Article on the web 17th February 2006
DOI: 10.1039/b515166j

We present a density functional theory study of the structure and reactivity of Pt(110) under high loads of atomic oxygen. Surface structures in which the oxygen adsorbs on PtO_2-like stripes along the Pt ridges of the Pt(110) are found to be highly stable. The structures become further stabilized when Pt atoms are ejected from the Pt ridges since this allows for stress relief along the PtO_2 stripes. Our results thus corroborate the Pt(110)-(12 × 2)-22O surface oxide structure proposed by Li *et al.* [*Phys. Rev. Lett.*, 2004, **93**, 146104]. We further considered the structure and stability of bulk α-PtO_2 oxide surfaces. The (0001) and (10$\bar{1}$0) facets are found to be the lowest energy facets. Finally, the reactivity of the surface oxide and the oxide surfaces in terms of CO oxidation was investigated. We find small energy barriers for the reaction at the Pt(110)-(12 × 2)-22O surface oxide and at the (10$\bar{1}$0) facet of α-PtO_2, but only large barriers over the α-PtO_2(0001) surface.

1. Introduction

Heterogeneous catalysts must generally fulfil two requirements: (i) provide low energy routes at their surfaces for the trapping of reactants, the formation of intermediate species, and the creation of reaction products, and (ii) be sufficiently benign in the bonding of the reactants, intermediates and products, that the surfaces do not become polluted. In oxidation reactions over supported metal particles, these requirements can be fulfilled in at least two ways: (1) the particles remain metallic, possibly highly covered with adsorbed oxygen atoms, and the reaction takes place in the adsorbate layers, or (2) the particles undergo oxidation in the outer regions, and the reaction takes place on the oxidized surface.

Advances in surface science characterization of transition metal surfaces under non-negligible partial pressures of oxygen, have recently led to the discovery of nano-scale thin films of oxides, *surface oxides*, on the surfaces of late transition metals such as Rh,[1–3] Pd,[4–7] Ag,[8] and Pt.[9] The surfaces of more reactive metal particles are expected to oxidize to a larger extent, *i.e.* not only in the outermost surface layers. On Ru surfaces thick layers of rutile, RuO_2(110), form already at 10^{-2} mbar of O_2 and T = 700 K and the model reaction of CO oxidation has been shown to run on the surface of this oxide using both experimental[10–12] and theoretical[13–15] methods.

Whether the thin surface oxides play a role under catalytic conditions is still to be investigated for most surfaces. So far, Hendriksen, Frenken, and co-workers[16,17] have shown that Pt(110) must reconstruct into one of several possible surface oxide structures to yield high O_2 + CO reaction rates. In their work, the activity of a Pt(110) model catalyst under near reaction conditions was measured, while the catalyst structure was monitored by scanning tunneling microscopy (STM)[16] and surface X-ray diffraction (SXRD)[17] techniques. The Pt(110) was exposed to O_2 and CO at different O_2/CO pressure ratios for total pressures up to 0.5 bar and temperatures of 425–625 K. The morphology of the Pt(110) surface was observed during CO oxidation and a strong correlation between the reactivity and the structure of the surface was identified. At 425 K and a low O_2/CO pressure ratio the reactivity is low and the surface exhibits a metallic state mainly covered by CO.[16] At a high O_2/CO pressure ratio the reactivity becomes significant and as a certain O_2/CO pressure ratio is surmounted, the reactivity increases abruptly followed by an immediate corrugation of the surface. This corrugation may be interpreted as oxide growth. The reverse phase transition occurs when the O_2/CO pressure ratio decreases again. At 625 K the growth of a transient oxide structure (commensurate with the surface and possibly containing $CO_3^{\delta-}$ species) was detected at high O_2/CO pressures ratios.[17] After some time, the structure changed into a rough, thin film of α-PtO_2. Both oxide structures were found to have substantially higher activity than the metallic Pt(110) surface. In a complementary study, Andersen and co-workers[18] showed how 1-D surface oxides confined to surface steps form under even milder conditions (10^{-6} Torr O_2, 310 K). The 1-D surface oxides were found to be more reactive in terms of reaction with co-adsorbed CO than the metallic surface covered with chemisorbed oxygen.

In the present paper we present a density functional theory study of the structure and reactivity of Pt with high oxygen loads. The structures of Pt(110) surfaces covered by up to 1.00 ML of oxygen are analyzed. For a large range of thermodynamic parameters (O_2 pressure and temperature) the surface is calculated to reconstruct into the Pt(110)-(12 × 2)-22O surface oxide structure proposed in ref. 9. The surface energies of various facets of Pt bulk oxide, α-PtO_2, are calculated and the (0001) and (10$\bar{1}$0) facets are identified as the most stable ones. Subsequently, the potential energy profiles for CO adsorption and reaction with oxygen are mapped out over the Pt(110)-(12 × 2)-22O surface oxide and over the two α-PtO_2 facets. It is found that the surface oxide is highly reactive

[a] *Interdisciplinary Nanoscience Center (iNANO) and Department of Physics and Astronomy, University of Aarhus, DK-8000 Aarhus C, Denmark. E-mail: hammer@phys.au.dk*
[b] *State Key Laboratory of Catalysis and Center for Theoretical and Computational Chemistry, Dalian Institute of Chemical Physics, Chinese Academy of Science, Dalian, 116023, China*

as is the α-PtO_2(10$\bar{1}$0) surface. The α-PtO_2(0001) facet, however, appears to be inert.

2. Calculation details

We perform first-principles total energy calculations within the DFT framework using the DACAPO code.[19–21] The Kohn–Sham wave functions are expanded in a plane wave basis (E_{cut} = 25 Ry) and the ionic cores are described by ultrasoft pseudopotentials[22] (with core cutoff radii of: r_c^C = 0.6, r_c^O 0.7, r_c^{Pt} = 1.2 a_0). All energies are calculated self-consistently approximating the exchange correlation part by the revised Perdew–Burke–Ernzerhof (RPBE) GGA functional,[19] but non-self-consistent energies based on the Perdew–Wang-91 (PW91) GGA functional[23] are included for consistency with the literature. The RPBE functional is used due to its more reliable molecular reaction and adsorption energetics.[19,24] All calculations, except for the reference O_2(g) calculation, are without spin polarization. In the case of the Pt(110) surface, the Brillouin zone is sampled by a (12/N × 2) Monkhorst–Pack (MP) **k**-point grid[25] for a (N × 2) super cell, and the surface is modeled by a five-layer-thick slab the two bottom layers of which are fixed in bulk positions and the rest are fully relaxed. Increasing the layer thickness from 5 to 9 stabilizes the 1 ML O covered Pt(110) by 40 meV per O. (We define 1 ML as one O per Pt(1 × 1) cell.) The binding energy of 0.5 ML CO on the 2 ML O covered surface is stabilized by 40 meV but the relative energy difference of CO adsorbed in the trough and on the ridge changes by less than 1 meV, which is consistent with previous studies.[26] The vacuum between slabs without CO adsorption is more than 10 Å. Increasing the vacuum by 5 Å changes the binding energy for CO adsorbed at the ridge (worst case scenario) by less than 20 meV.

In the case of α-PtO_2, we sample the Brillouin zone of the (0001) surface by 18 special **k**-points[27] for a (2 × 2) cell. Because of the weak van der Waals interaction between the trilayers of α-PtO_2, it is sufficient to consider only one layer when investigating the reactivity of the (0001) surface. A two layer slab changes the heat of formation of an oxygen vacancy and the binding energy of a CO molecule by less than 5 and 15 meV, respectively. For the facets (10$\bar{1}$0), (10$\bar{1}$1), and (2$\bar{1}\bar{1}$0) we have employed a (6 × 2) Monkhorst–Pack (MP) grid for the (1 × 1) cells. When calculating CO adsorption and oxidation on the (10$\bar{1}$0) surface, a 4 layers thick (2 × 2) slab is used and the Brillouin zone is sampled by a (4 × 2) MP grid. Increasing the slab from 4 to 6 layers changes the heat of formation of an oxygen vacancy and the binding energy of a CO by *ca.* 4 meV.

3. Experimental background

3.1. Pt(110) surface oxide

Pt(110) has been investigated intensively with surface science techniques. The energetically favored structure of the clean Pt(110) surface is known from low energy electron diffraction (LEED)[28] and medium energy ion scattering[29] studies to be the (1 × 2) missing-row reconstruction where every second [1$\bar{1}$0] row is missing. In the presence of adsorbed atomic oxygen, the metal surface retains its reconstruction from low to high coverage.[26,30] In contrast to this, exposure to CO causes the lifting of the reconstruction.[31–33] The O adsorbs along the ridges and at *ca.* 1 ML the ridges become saturated (1 ML = one O per Pt(1 × 1) cell). At this coverage the ridges resemble the PtO_2 rows in bulk PtO_2 and we shall refer to them as "PtO_2 rows" (or "PtO_2 stripes" when they are segmented). Before the surface becomes saturated, STM images show that patches of a local *ca.* 1 ML O coverage (finite PtO_2 stripes) occur.[26,30] If the temperature is high enough to ensure thermodynamic equilibrium, the (1 × 2) surface reconstructs further into a (N × 2) super structure, $N \simeq 12$, where two out of every N Pt atoms in the PtO_2 rows are ejected.[9]

3.2. α-PtO_2

The alpha platinum dioxide, α-PtO_2, consists of sheets of hexagonal PtO_2 tri-layers separated by more than 4 Å and has a structure which is similar to that of CdI_2.[34] The oxide shows poor crystallinity and single crystal α-PtO_2 has, to our knowledge, not been observed so far. McBride *et al.*[35] produced thin α-PtO_2 films *via* sputtering and determined from X-ray diffraction (XRD) the lattice parameters a = 3.113 and c = 4.342 Å. The poor crystallinity is seen from the lack of order in the c direction as confirmed by Zhensheng *et al.*,[36] who produced α-PtO_2 powder by a fusion method and also found by XRD the lattice parameters a = 3.10 and c = 4.29–4.41 Å. Transmission electron microscopy (TEM) images were taken that showed needle-like micro-crystals of *ca.* 6 nm diameters and *ca.* 50 nm length.

4. Structure determination

4.1. Pt(110) surface oxide

The Pt(110) surfaces with and without adsorbed atomic oxygen considered in our study are shown in Fig. 1. For the clean Pt(110) we calculate in agreement with other theoretical findings[37] an energy difference of 0.18 eV per (1 × 2) unit area between the reconstructed, Fig. 1a, and un-reconstructed structures, Fig. 1b. The reconstructed surface is the preferred one.

Introducing adsorbed atomic oxygen, we have tested a number of adsorption geometries. At 0.25 ML coverage, the oxygen adsorbs at the bridge sites on the ridge (not shown) while it is 0.04 eV less favorable per oxygen to occupy FCC sites on the inclined (111) nano-facets on the sides of the ridge. At 0.5 and 1.0 ML, Fig. 1(c–d), the atomic oxygen adsorbs preferentially in the FCC sites with chemisorption potential energies of −0.75 and −0.69 eV per O.

Inspired by the experimental observation in ref. 9 and 26 of local *ca.* 1 ML oxygen structures on the Pt(110) ridges we further considered the configurations shown in Fig. 1(e–h). In these models, stripes of PtO_2 units are becoming longer and longer in super cells of an arbitrarily fixed length, namely six Pt nearest neighbor distances in the [1$\bar{1}$0] direction. The total oxygen coverage increases from 0.33 to 0.83 ML. The adsorption potential energies per oxygen decrease slightly (numerically) from −0.75 eV at 0.33 ML to −0.72 eV at 0.83 ML oxygen. Expansion within the PtO_2 stripes (and contraction within the bare parts of the Pt ridges) reveal that stress relief is

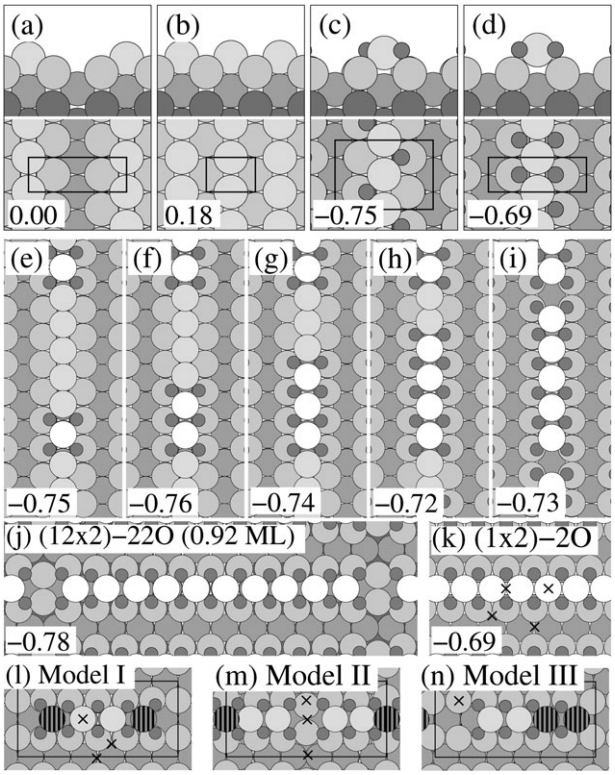

Fig. 1 (a–b) Clean Pt(110) structures: the numbers refer to the formation energies (in eV) of the surface per (1 × 2) unit area with respect to the reconstructed surface. (a) The reconstructed and (b) unreconstructed Pt(110) surface. (c–n) Oxidized Pt(110) structures: the formation energies (in eV) per O are given. (c) Pt(110)-(2 × 2)-2O (0.5 ML). (d) Pt(110)-(1 × 2)-2O (1.0 ML). (e) Pt(110)-(6 × 2)-4O (0.33 ML). (f) Pt(110)-(6 × 2)-6O (0.50 ML). (g) Pt(110)-(6 × 2)-8O (0.67 ML). (h) Pt(110)-(6 × 2)-10O (0.83 ML). (i) Pt(110)-(6 × 2)-12O, (1.00 ML, one ridge Pt atom ejected). (j) Pt(110)-(12 × 2)-22O, (0.92 ML, two ridge Pt atoms ejected). (k) Same as (d). (l–n) Pt(110)-(6 × 2) models I–III of part of the structure in (j). In (f–j) the average Pt–Pt expansions within the PtO_2 stripes are: 8.1, 5.6, 4.2, 7.0, and 8.1%, respectively. The crosses indicate the CO adsorption sites.

the driving force for the stripe segmentation. The Pt–Pt separation within the PtO_2 stripes thus expands in the order of 4–8%. Similar structures have been observed and characterized on Rh(110).[38] Guided further by the observation with STM of ejection of Pt atoms from the bare parts of the Pt ridges, we considered two high oxygen coverage structures in which Pt atoms were moved from the Pt ridge to Pt bulk sites in separate calculations. Ejecting every sixth Pt atom from the ridge at 1 ML oxygen coverage, Fig. 1i, results in an energy gain of about 0.04 eV per oxygen atom. Again, the reason for the energy gain appears to be stress relief as the Pt–Pt distance within the stripes is calculated to increase by 7%. Ejecting two adjacent Pt ridge atoms for every twelve Pt atoms results, at 0.92 ML oxygen (Fig. 1j), in an energy gain of 0.09 eV per oxygen atom and in considerable expansion of the Pt–Pt separation (8.1%). This latter structure must formally be named Pt(110)-(12 × 2)-22O according to the naming convention for chemisorption structures. However, we consider the structures involving ejection of Pt atoms to be more than just chemisorption structures, and refer to them below as Pt(110) *surface oxide* models.

Based on the oxygen chemisorption structures and surface oxide models in Fig. 1 we have constructed the surface free energy diagram, Fig. 2, for Pt(110) in the presence of an O_2 gas. The thermodynamic parameters of the O_2 gas are described by the chemical potential, $\Delta\mu_O$. The O_2 partial pressures corresponding to $\Delta\mu_O$ at a temperature of 300 K are shown in the figure. The shaded background in the diagram marks the range of $\Delta\mu_O$ where bulk α-PtO_2 is thermodynamically favored ($\Delta\mu_O > {}^1/_2\Delta E_{PtO_2}$—see below). In agreement with STM experiments[9] we find the Pt(110)-(12 × 2)-22O surface oxide to be energetically favorable in a large range of $\Delta\mu_O$. We note, however, that since we have only considered Pt(110)-(N × 2) structures for N = 2, 6, and 12, the present study does not allow for an exact identification of the most favorable value of N. The calculated expansion within the PtO_2 stripes of this structure is only 8% on average as opposed to a measured 14% expansion.[9] The calculated 8% expansion corresponds to an average Pt–Pt distance of 3.08 Å. (Incidentally, this is similar to the Pt–Pt distance of 3.05 Å of a free PtO_2 row.[18]) The calculated expansion is not uniform but increases from a 6% expansion in the middle areas to almost 11% expansion at the end areas. It should be noted that the measured expansion relies on assignment of bright STM protrusions to atomic Pt positions, which need not be a safe choice.

Given the high stability of the Pt(110)-(12 × 2)-22O surface oxide we will be modeling the reactivity of this surface below. In order to make the calculations feasible, we built some

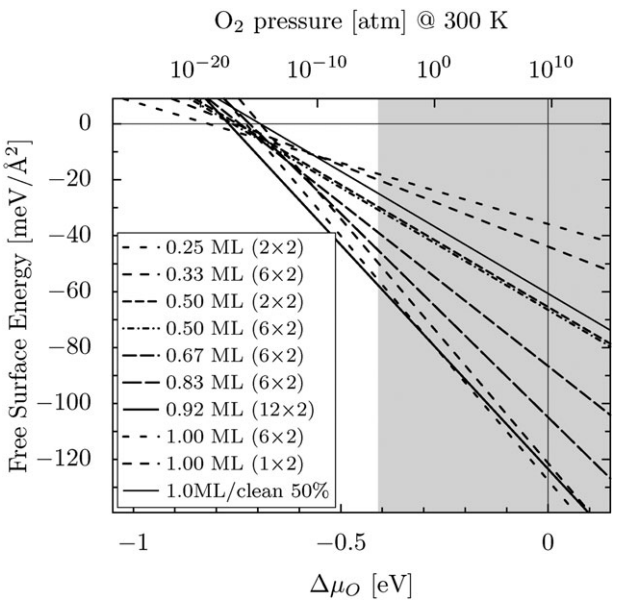

Fig. 2 Free surface energy diagram. The reference is the clean (1 × 2) reconstructed Pt(110) surface depicted in Fig. 1a. The legends refer in order of appearance to the structures: 1. 0.25 ML O in bridge sites along the Pt-ridge; 2. Fig. 1e; 3. Fig. 1c; 4. Fig. 1f; 5. Fig. 1g; 6. Fig. 1h; 7. Fig. 1j; 8. Fig. 1i; 9. Fig. 1d and k; 10. a reconstructed surface covered 50% by large islands of the 1 ML structure, Fig. 1d. The shaded area identifies the region where bulk α-PtO_2 is thermodynamically preferred.

smaller (6 × 2) models of parts of the surface oxide. These models, I–III, are shown in Fig. 1(l–n), where hatched atoms are constrained in some dimensions. Models I and II are meant for studying the middle and terminal parts of the PtO_2 stripes in the continuous (12 × 2) reconstruction, while model III is built to enable the modeling of the reactivity at the phase boundary between the (12 × 2) reconstructed island and a bare (or CO covered) metallic part of the Pt(110) surface. In order to assess the accuracy of the (6 × 2) models, we list in Table 1 the differential adsorption potential energies of the atomic oxygen either in the middle of stripes or at the end of stripes. The *differential* adsorption potential energy is minus the energy it takes to form $1/2O_2$ from one oxygen in the structure leaving behind a vacancy. From the table, it is seen that oxygen atoms in both the (1 × 2)-2O (modeled in a (2 × 2) cell) and (6 × 2)-I structures are reasonable models for oxygen atoms in the middle of the (12 × 2)-22O surface oxide stripes. Also, the oxygen atoms in the (6 × 2)-II model constitute fair models of the oxygen atoms at the ends of the (12 × 2)-22O surface oxide stripes.

4.2. α-PtO_2

For the α-PtO_2 bulk oxide we calculate a formation energy of $\Delta E_{PtO_2} = -0.82$ eV per PtO_2 unit. Since the DFT approach lacks a proper description of van der Waals forces, the inter-layer separation between the hexagonal PtO_2 sheets becomes too large, $c = 5.30$ Å, compared to experiment. The strong bonding within the sheets is, however, well described and the calculated lattice parameter, $a = 3.20$ Å, is consequently in good agreement with experiment. The Pt–O bond length is found to be 2.09 Å slightly longer than the 2.05–2.06 Å calculated for the Pt(110)-(1 × 2)-2O structure (Maya *et al.*[39] and Dai *et al.*[40] find 2.01 and 2.03 Å, respectively).

In order to select for our reaction studies the facets that are the predominant ones for thick PtO_2 films or PtO_2 crystallites, we have calculated the surface energies (Table 2) of some low index facets shown in Fig. 3a–d. Because the interaction between the tri-layers is of van der Waals character, the calculated surface energy of (0001) is almost zero. The two most low-index facets orthogonal to (0001) are $(10\bar{1}0)$ and $(2\bar{1}\bar{1}0)$. From the surface energies of these two facets we have produced a 2-D Wulff construction, Fig. 3e, from which we conclude that the only stable facets orthogonal to the (0001) are the $(10\bar{1}0)$ facets. As a further consequence of the vanishing inter-layer interaction in the (0001)-direction the surface energy per surface Pt atom for the $(10\bar{1}1)$ facet becomes very similar to that of the $(10\bar{1}0)$ facet.

Table 1 Differential adsorption potential energies for oxygen atoms with respect to $1/2O_2$

Site	RPBE (PW91)
O in middle of stripe:	
(2 × 2)	−0.96 (−1.25)
(12 × 2)	−1.15 (−1.48)
(6 × 2)-I	−1.43 (−1.76)
O at end of stripe:	
(12 × 2)	−1.18 (−1.48)
(6 × 2)-II	−1.20 (−1.56)
(6 × 2)-III	−0.80 (−1.06)

Table 2 Unit cell areas, surface energies, E, per unit cell area, and surface energies, γ, per Å^2 for low index PtO_2 facets

Facet	(0001)	$(10\bar{1}0)$	$(2\bar{1}\bar{1}0)$	$(10\bar{1}1)$
Area/Å^2	8.868	17.12	29.65	19.95
E/eV	0.006	1.32	2.88	1.32
γ/meV Å^{-2}	0.7	77.1	97.1	66.1

5. Reactivity

In this section we address the reactivity of the oxidized Pt(110) and α-PtO_2 with respect to CO oxidation. We are searching for the minimum potential energy path (MEP) taking us from CO(g) + the oxidized surface to CO_2(g) + the surface with a vacancy. The replenishment of the vacancy with oxygen is assumed to be a facile step and will not be studied. The CO oxidation step can happen either through the Eley–Rideal (ER) mechanism in which the CO reacts directly from the gas phase with an oxygen atom from the surface or *via* the Langmuir–Hinshelwood (LH) mechanism in which the CO adsorbs, diffuses and finally reacts with an adsorbed oxygen atom.[41] If the LH mechanism requires an oxygen vacancy in the oxide surface to proceed, it is also called a Mars van Krevelen mechanism.[42] Different methods are used at different stages along the MEP. We preferably employ the *drag method*, where the O–CO distance is used as the reaction coordinate,[43] but when this fails we apply the *nudged elastic band method* (NEB). In the NEB method the (approximate) distance along the MEP is used as the reaction parameter.[44,45] Care has been taken that the paths are continuous.

5.1. Pt(110)

Exposed only to CO the reconstruction of the bare Pt(110) is known experimentally to be lifted gradually at CO coverages somewhere between 0.2 and 0.5 ML.[31–33] Gritsch *et al.* report $\theta_{CO} \simeq 0.2$ ML as the critical CO coverage at room temperature where (1 × 1) patches start to form.[32] At $\theta_{CO} \simeq 0.5$ ML the transformation is complete. We calculate in accordance

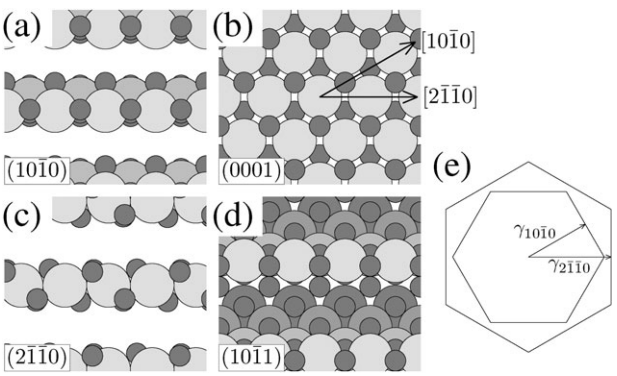

Fig. 3 (a–d) Four different α-PtO_2 facets and (e) the 2-D Wulff construction for surfaces orthogonal to the (0001) facet. The PtO_2 rows in the topmost layer of (a) and (d) are calculated to be rotated 43 and 64°, respectively, with respect to the orientation of the subsurface PtO_2 rows.

with the experimental findings that the reconstructed surface is more stable than the unreconstructed surface at $\theta_{CO} \simeq 0.25$ ML and *vice versa* at $\theta_{CO} \simeq 0.5$ ML. The 1 ML saturated surface exhibits a (2×1)-*p*1*g*1 structure where the COs are adsorbed atop and tilted in an alternating fashion along the ridges[46,47] (we calculate the tilting to release about 0.05 eV per CO). In a mixed CO and O_2 environment, structures with both species adsorbed are expected. The individual coverages depend on the ratio of the chemical potentials. In this paper we assume that the Pt(110) supports the (12×2)-22O surface oxide discussed above, even when exposed to some amount of CO.

We begin by modelling the surface oxide by the Pt(110)-(1×2)-2O structure in (2×2) cells. This model is small and hence computationally efficient, but lacks the stress relief present in the true surface oxide. The crosses in Fig. 1k indicate the different CO adsorption sites over the (1×2)-2O structure, and the associated adsorption potential energies and bond lengths are tabulated in Table 3. That the (2×2) cell is large enough for the CO molecules not to interact through the periodic boundary conditions was checked by varying the cell size: adsorption potential energies of CO in the trough bridge site are −0.17, −0.41, and −0.47 eV (PW91: −0.72, −0.91, −0.98 eV) calculated in (1×2), (2×2), and (3×2) unit cells, respectively.

In Fig. 4(a–b) we display the potential energy with respect to CO in the gas phase at certain points along the LH and ER reaction pathways on the Pt(110)-(1×2) surface. For the adsorption of CO, we employed both the NEB and the drag method and made sure the adsorption path was asymmetric. In both cases we find an adsorption barrier of 0.5 eV and the transition state is reached when the carbon atom is at the same height as the PtO_2 row (left-most structure in Fig. 4a). The most stable adsorption site is the long bridge site in the trough where the two Pt atoms bonding to the CO are pulled towards the CO. In the transition state towards CO_2 formation, the CO is adsorbed in an atop site of the inclined (111) nano-facet of the ridge and the nearest O is pushed upwards and slightly away from the CO. The CO bond length is reduced by 0.02 Å compared to the CO adsorbed in the trough, the O–CO distance is 2.20 Å, and the bond angle, $\angle_{O-CO}$, is 103°. This geometry is very similar to that of the CO reaction with adsorbed O on Pt(111), as described by Alavi *et al.*[48] and Eichler and Hafner.[49] The CO oxidation barrier, however, is only 0.3 eV which is more than 0.4 eV smaller than for the reaction on Pt(111). Before the final desorption of the CO_2 it passes through a weak physisorption state with a desorption barrier less than 0.02 eV. For the ER reaction we calculate a much higher CO oxidation barrier than in the LH case. The geometry of the transition state corresponds to a CO_2 molecule with one elongated (1.66 Å) and one short (1.17 Å) bond and a bond angle of 126°. Again this geometry resembles very much the geometry of the transition state of the corresponding reaction on Pt(111).[48,49]

We now turn to the CO oxidation reaction on the (6×2) models of the Pt(110)-(12×2)-22O surface oxide. The CO adsorption sites are indicated in Fig. 1(l–n) and numbers are listed in Table 3. The most stable site in model I is the long bridge site in the trough. This is not surprising since this part of the (12×2) structure resembles the (1×2) structure. We also note that the adsorption on every site has been stabilized by approximately 0.3 eV which is explained by the expansion of the PtO_2 row.[50] Moving to model II, CO adsorption becomes thermo-neutral if not endothermic when the adsorption sites are chosen in the region where Pt atoms have been ejected between the PtO_2 stripes. The reason for this may be that most of the relaxation of the substrate near the boundary of two stripes is destroyed upon CO adsorption. The most stable site is the atop site where the CO is tilted 23° towards the trough. Finally, using model III for the boundary between a PtO_2 stripe island and the reduced (1×1) surface, it is found that away from the oxide stripes, the CO binding energies quickly approach those on the pure Pt(110)-(1×1) surface.

The potential energy profile of the CO adsorption and the LH oxidation reaction on model I plotted in Fig. 4c is almost

Table 3 RPBE adsorption potential energies (in parenthesis: PW91 based values) and geometrical values: CO bond length (d_{CO}), O–CO bond length (d_{O-CO}), and C–Pt distance (d_{C-Pt}). The energy zero is the sum of the total energies of CO(g) and the surfaces in separate calculations

	E/eV	d_{CO}/Å	d_{O-CO}/Å	d_{C-Pt}/Å
Pt(110)-(1 × 2)				
TS(ads)	0.49 (0.11)	1.159		
Trough bridge	−0.41 (−0.91)	1.185		2.056
Trough fcc	−0.29 (−0.79)	1.181		2.058
Ridge atop	0.16 (−0.18)	1.162		1.967
Ridge bridge	0.52 (0.15)	1.164		1.974
O · CO complex	−1.02 (−1.43)	1.209	1.341	2.037
TS(LH)	−0.10 (−0.51)	1.163	2.204	1.900
TS(ER)	1.20 (0.92)	1.173	1.660	
Pt(110)-(6 × 2)-I				
TS(ads)	0.25 (−0.07)	1.158		
Trough bridge	−0.74 (−1.22)	1.188		2.049
Trough fcc	−0.60 (−1.07)	1.187		2.035
Ridge atop	−0.17 (−0.45)	1.160		1.957
TS(LH)	−0.47 (−0.87)	1.168	2.010	1.910
O · CO complex	−1.25 (−1.63)	1.207	1.356	2.015
TS(ER)	0.99 (0.75)	1.178	1.599	
Pt(110)-(6 × 2)-II				
Atop	−0.02 (−0.45)	1.162		1.894
Trough bridge	0.15 (−0.24)	1.186		2.096
Short bridge	0.27 (−0.22)	1.184		2.002
TS(LH)	0.07 (0.05)	1.169	2.007	1.926
Pt(110)-(6 × 2)-III				
Atop	−1.41 (−1.82)	1.167		1.882
TS(LH)	−1.14 (−1.61)	1.179	1.900	1.940
α-PtO_2(0001)				
TS(ads)	1.78 (1.89)			
O · CO complex	−0.39 (−0.82)	1.198	1.341	2.052
α-PtO_2(0001)-vac				
TS(ads)	0.74 (0.38)	1.162		
Bridge	−0.53 (−0.99)	1.194		2.078
Subst.	−0.24 (−0.72)	1.197		2.200
TS(LH)	1.43 (1.49)	1.162	2.609	1.906
O · CO complex	−0.82 (−1.24)	1.202	1.368	2.035
α-PtO_2(10$\bar{1}$0)				
TS(ads)	0.10 (0.02)			
Atop	−1.41 (−1.86)	1.156		1.918

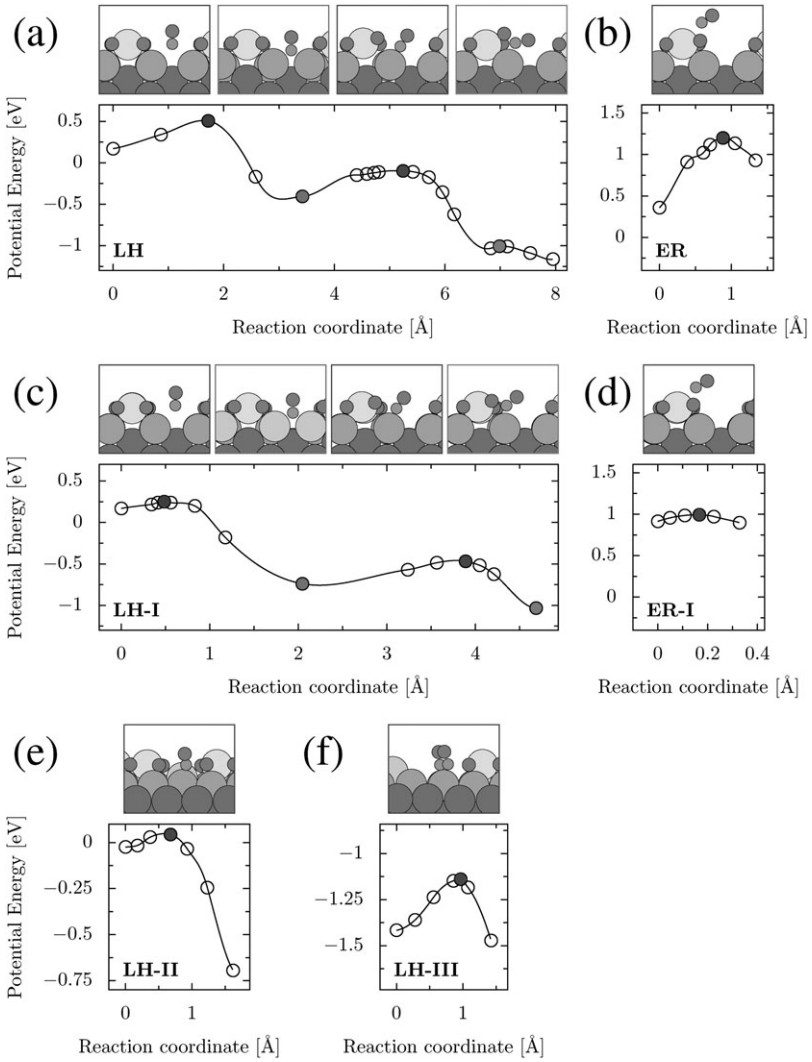

Fig. 4 CO oxidation on models of the surface oxide covered Pt(110). The energy zero is for CO far from the surfaces. (a) CO adsorption and subsequent oxidation *via* a LH type reaction on Pt(110)-(1 × 2)-2O modeled in a (2 × 2) cell. (b) oxidation *via* an ER mechanism on the same surface. (c–f) CO oxidation on Pt(110)-(12 × 2)-22O using models I–III. (c) Model I: CO adsorption and subsequent oxidation *via* a LH type reaction. (d) Model I: oxidation *via* the ER mechanism. (e) Model II: LH type oxidation of CO between two stripes. (f) Model III: LH oxidation of CO adsorbed at the boundary of the CO saturated (1 × 1) surface and the (12 × 2) oxide surface.

identical to that of the LH energy diagram of the (1 × 2) structure, Fig. 4a, except for a general 0.3 eV stabilization of all geometries. Since the reference energy of CO in the gas phase is unaffected by whether the PtO_2 stripe is expanded or not, the overall reaction barrier dictated by the adsorption barrier is lowered by approximately 0.3 eV. The same effect is seen for the ER reaction, Fig. 4d.

The reaction paths and energy profiles for the CO oxidation reaction at the boundaries between two PtO_2 stripes (model II) and a PtO_2 stripe and reduced (1 × 1) surface (model III) are shown in Fig. 4e–f. In the former case, the CO oxidation barrier is only 0.1 eV, so if the CO adsorption barrier at the boundary is similar to the one in the middle of the PtO_2 stripe the reaction channel seems very promising. The three-phase boundary structure of model III turns out to be quite reactive also in agreement with our previous findings for a related setup on Pt(111).[51] We assume that the CO readily adsorbs and diffuses on the clean Pt(110) and we have therefore not calculated any adsorption barriers. The oxidation barrier of the CO reacting with an oxygen atom from the end of the PtO_2 stripe is again only 0.3 eV. Because the present LH reaction barriers are so low whereas the ER reactions so far have had high barriers, we did not calculate the ER reaction pathways for models II and III.

5.2. α-PtO_2

We begin by considering CO adsorption on the α-PtO_2(0001) surface, *cf.* Table 3. For adsorption on the pristine surface we find only one energy minimum which is realized by forming a O · CO surface complex. Next, we prepare a defected α-PtO_2(0001) surface by introducing oxygen vacancies. The results for subsequent CO adsorption given in Table 3 show that CO is stabilized by the vacancy. The stabilization is, however, much smaller than the vacancy formation energy

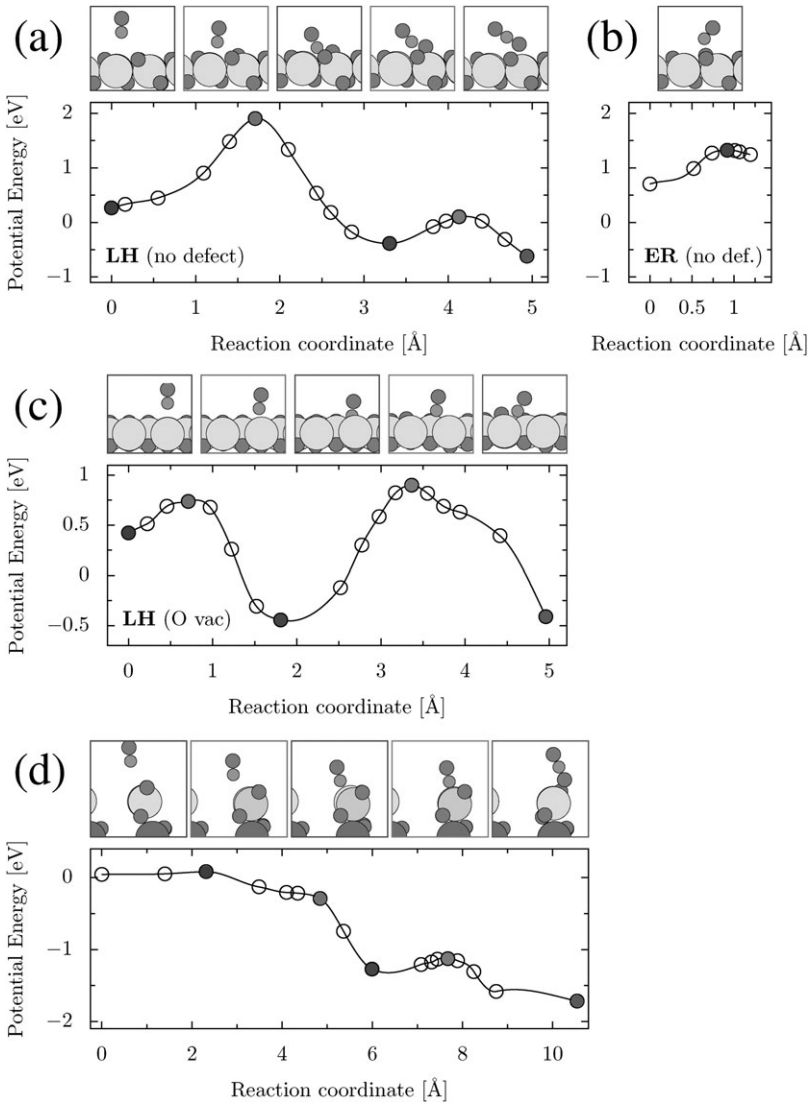

Fig. 5 CO oxidation *via* (a) LH and (b) ER pathways on the pristine α-PtO_2(0001). (c) LH (or Mars van Krevelen) reaction pathway for CO on α-PtO_2(0001) with a preexisting oxygen vacancy. (d) Adsorption and oxidation of CO on the (10$\bar{1}$0) facet of α-PtO_2. In all subfigures, the energy zero is for CO far from the surfaces.

which we calculate to be substantial; 1.67 eV. The CO adsorbs either in a Pt–Pt bridge site adjacent to the vacancy or substitutionally, *i.e.* in the vacancy.

For the perfect α-PtO_2(0001) surface, we plot in Fig. 5a the reaction potential energy diagram for the CO adsorption and oxidation reactions. It is seen that the adsorption of the CO on the pristine surface is a highly activated process with an energy barrier of 1.9 eV. The following oxidation of the CO involves a more modest barrier of 0.5 eV. Likewise, the ER reaction, Fig. 5b, also involves large barriers. Overall, CO oxidation on the (0001) surface is unlikely. Turning to the surface with defects, Fig. 5c, we again calculate a considerable CO adsorption barrier of 0.74 eV. From the bridge site the CO moves to one of the nearest oxygen atoms, over one of the Pt atoms to which it bonds. Here it forms the more stable O · CO complex, identical to the O · CO complex found on the pristine surface. This diffusion is associated with another huge reaction barrier of 1.4 eV proving yet again the (0001) surface to be considerably *non*-reactive.

Finally, we consider in Fig. 5d the (10$\bar{1}$0) surface. Contrary to the (0001) surface this surface adsorbs CO readily with an adsorption barrier of less than 0.1 eV. The CO binding energy of 1.4 eV on the (10$\bar{1}$0) is the largest of all the surfaces considered in this study. The following oxidation reaction barrier of the CO is only 0.3 eV meaning that the overall reaction on this facet appears to be facile.

5.3. Discussion

Our findings of small reaction barriers for the CO oxidation on the Pt(110)-(12 × 2)-2O surface oxide and on the open α-PtO_2(10$\bar{1}$0) surface are in qualitative agreement with the experiments by Hendriksen, Frenken, and co-workers.[16,17] In their first experiment, the reactive state of Pt(110) at 425 K was seen by STM to involve a grainy surface morphology, which was discussed as possible oxide formation. In their second experiment, the most active surface structure at higher temperatures, 625 K, was determined by SXRD to involve a few

tri-layers of α-PtO_2. If the grainy structures in the first experiments are oxide crystallites, then they must contain the $(10\bar{1}0)$ facets according to topological reasoning (the Wulff construction). Likewise, it is realized that edges of $(10\bar{1}0)$ character must exist in the second experiment.[17] This is a consequence of the roughness of the α-PtO_2 film, which was found to consist of a *non-integer* number of tri-layers. A rough film most likely consists of islands of α-PtO_2(0001) sheets, the perimeters of which will be $(10\bar{1}0)$ type steps. The high reactivity of the $(10\bar{1}0)$ facet calculated in this work thus rationalizes the observation in both experiments of high catalytic activities under high O pressures. We note, however, that since we also calculate the Pt(110)-(12 × 2)-22O surface oxide to be reactive, we cannot rule out that the reaction simply takes place on the regions of the surface covered by this structure. This would in particular be relevant to the low temperature experiment where no structure determination was done,[16] and would explain why no increase in the activity was measured despite that the size of the grainy structures increased with time[16]—a fact that could, however, also be explained in terms of the overall reaction rate being limited by the flow rate of the whole reactor unit.

6. Conclusions

In conclusion, we have presented a density functional theory study of the structure and reactivity of Pt(110) under high oxygen coverages. The oxygen is found to form PtO_2 stripes along the Pt ridges of the Pt(110) surface. The stripes expand and the stress relief is sufficiently large that Pt atoms are ejected from between the PtO_2 stripes. Constructing the surface free energy phase diagram, the experimentally proposed Pt(110)-(12 × 2)-22O surface oxide structure[9] is found to be favorable for a large region of oxygen chemical potentials when compared to a large number of alternative structures in (2 × 2) and (6 × 2) cells.

To determine the surface structure after further oxidation of the Pt(110) the most stable surfaces of bulk α-PtO_2 crystals were identified by calculation of surface energies. Based on this, the (0001) and $(10\bar{1}0)$ facets were argued to be the most abundant facets for large α-PtO_2 crystallites. A large structural relaxation was found for the outermost PtO_2-row in the open, $(10\bar{1}0)$ facet.

Finally, the reactivity of the surface oxide and the oxide surfaces was investigated. As a model reaction, the oxidation of CO with lattice O was investigated. Depending on the model used, barriers of the order of 0.25 eV were found for the adsorption of CO and the formation of CO_2 over the Pt(110)-(12 × 2)-22O surface oxide. The open oxide surface, α-$PtO_2(10\bar{1}0)$, also showed large affinity towards binding CO and no appreciable barriers for the CO adsorption and CO oxidation. On the α-PtO_2(0001) hexagonal basal planes the only CO adsorption pathway involved direct formation of a O·CO surface complex. Introducing oxygen vacancies in the α-PtO_2(0001) surface provided, however, a CO adsorption state. In both cases, the barrier for the O·CO surface complex formation remained very large, no less than 1.4 eV. The α-PtO_2(0001) surface thus appears inert based on our calculations.

Acknowledgements

This work was financially supported by the Danish Research Council and Dansk Center for Scientific Computing. W. X. Li further thanks NFSC (20503030) for support.

References

1 J. Gustafson, A. Mikkelsen, M. Borg, E. Lundgren, L. Köhler, G. Kresse, M. Schmid, P. Varga, J. Yuhara, X. Torrelles, C. Quirós and J. N. Andersen, *Phys. Rev. Lett.*, 2004, **92**, 126102.
2 L. Kohler, G. Kresse, M. Schmid, E. Lundgren, J. Gustafson, A. Mikkelsen, M. Borg, J. Yuhara, J. N. Andersen, M. Marsman and P. Varga, *Phys. Rev. Lett.*, 2004, **93**, 266103.
3 J. Gustafson, A. Mikkelsen, M. Borg, J. N. Andersen, E. Lundgren, C. Klein, W. Hofer, M. Schmid, P. Varga, L. Kohler, G. Kresse, N. Kasper, A. Stierle and H. Dosch, *Phys. Rev. B*, 2005, **71**, 115442.
4 E. Lundgren, G. Kresse, C. Klein, M. Borg, J. N. Andersen, M. De Santis, Y. Gauthier, C. Konvicka, M. Schmid and P. Varga, *Phys. Rev. Lett.*, 2002, **88**, 246103.
5 M. Todorova, E. Lundgren, V. Blum, A. Mikkelsen, S. Gray, J. Gustafson, M. Borg, J. Rogal, K. Reuter, J. N. Andersen and M. Scheffler, *Surf. Sci.*, 2003, **541**, 101–112.
6 E. Lundgren, J. Gustafson, A. Mikkelsen, J. N. Andersen, A. Stierle, H. Dosch, M. Todorova, J. Rogal, K. Reuter and M. Scheffler, *Phys. Rev. Lett.*, 2004, **92**, 046101.
7 A. Stierle, N. Kasper, H. Dosch, E. Lundgren, J. Gustafson, A. Mikkelsen and J. N. Andersen, *J. Chem. Phys.*, 2005, **122**, 044706.
8 C. I. Carlisle, D. A. King, M. L. Bocquet, J. Cerdá and P. Sautet, *Phys. Rev. Lett.*, 2000, **84**, 3899.
9 W. X. Li, L. Österlund, E. K. Vestergaard, R. T. Vang, J. Matthiesen, T. M. Pedersen, E. Lægsgaard, B. Hammer and F. Besenbacher, *Phys. Rev. Lett.*, 2004, **93**, 146104.
10 H. Over, Y. D. Kim, A. P. Seitsonen, S. Wendt, E. Lundgren, M. Schmid, P. Varga, A. Morgante and G. Ertl, *Science*, 2000, **287**, 1474.
11 Y. D. Kim, H. Over, G. Krabbes and G. Ertl, *Top. Catal.*, 2001, **14**, 95.
12 S. H. Kim and J. Wintterlin, *J. Phys. Chem. B*, 2004, **108**, 14565.
13 K. Reuter and M. Scheffler, *Phys. Rev. B*, 2001, **65**, 035406.
14 K. Reuter and M. Scheffler, *Phys. Rev. Lett.*, 2003, **90**, 046103.
15 K. Reuter and M. Scheffler, *Phys. Rev. B*, 2003, **68**, 045407.
16 B. L. M. Hendriksen and J. W. M. Frenken, *Phys. Rev. Lett.*, 2002, **89**, 046101.
17 M. D. Ackermann, T. M. Pedersen, B. L. M. Hendriksen, O. Robach, I. Bobaru, I. Popa, H. Kim, B. Hammer, S. Ferrer and J. W. M. Frenken, *Phys. Rev. Lett.*, 2005, **95**, 255505.
18 J. G. Wang, W. X. Li, M. Borg, J. Gustafson, A. Mikkelsen, T. M. Pedersen, E. Lundgren, J. Weissenrieder, J. Klikovits, M. Schmid, B. Hammer and J. N. Andersen, *Phys. Rev. Lett.*, 2005, **95** 256102.
19 B. Hammer, L. B. Hansen and J. K. Nørskov, *Phys. Rev. B*, 1999, **59**, 7413–7421.
20 S. R. Bahn and K. W. Jacobsen, *Comput. Sci. Eng.*, 2002, **41**, 56.
21 http://www.camp.dtu.dk/campos.
22 D. Vanderbilt, *Phys. Rev. B*, 1990, **41**, 7892–7895.
23 J. P. Perdew, J. A. Chevary, S. H. Vosko, K. A. Jackson, M. R. Pederson, D. J. Singh and C. Fiolhais, *Phys. Rev. B*, 1992, **46**, 6671–6687.
24 S. Kurth, J. P. Perdew and P. Blaha, *Int. J. Quantum Chem.*, 1999, **75**, 889–909.
25 H. J. Monkhorst and J. D. Pack, *Phys. Rev. B*, 1976, **13**, 5188–5192.
26 S. Helveg, H. T. Lorensen, S. Horch, E. Lægsgaard, I. Stensgaard, K. W. Jacobsen, J. K. Nørskov and F. Besenbacher, *Surf. Sci.*, 1999, **430**, L533.
27 D. J. Chadi and M. L. Cohen, *Phys. Rev. B*, 1973, **8**, 5747–5753.
28 P. Fery, W. Moritz and D. Wolf, *Phys. Rev. B*, 1988, **38**, 7275.
29 P. Fenter and T. Gustafsson, *Phys. Rev. B*, 1988, **38**, 10197.
30 A. V. Walker, B. Klotzer and D. A. King, *J. Chem. Phys.*, 1998, **109**, 6879.
31 S. Ferrer and H. P. Bonzel, *Surf. Sci.*, 1982, **119**, 234.

32 T. Gritsch, D. Coulman, R. J. Behm and G. Ertl, *Phys. Rev. Lett.*, 1989, **63**, 1086–1089.
33 C. J. Baily, M. Surman and A. E. Russell, *Surf. Sci.*, 2003, **523**, 111–117.
34 C. Soulard, X. Rocquefelte, S. Jobic, D. Dai, H. Koo and M.-H. Whangbo, *J. Solid. State Chem.*, 2003, **175**, 353–358.
35 J. McBride, G. Graham, C. Peters and W. Weber, *J. Appl. Phys.*, 1991, **69**, 1596–1604.
36 J. Zhensheng, X. Chanjuan, Z. Qingmei, Y. Feng, Z. Jiazheng and X. Jinzhen, *J. Mol. Catal. A: Chem.*, 2003, **191**, 61–66.
37 S. Baud, C. Ramseyer, G. Bihlmayer, S. Blugel, C. Barreteau, M. C. Desjonqueres, D. Spanjaard and N. Bernstein, *Phys. Rev. B*, 2004, **70**, 235423.
38 E. Vesselli, C. Africh, A. Baraldi, G. Comelli, F. Esch and R. Rosei, *J. Chem. Phys.*, 2001, **114**, 4221–4225.
39 L. Maya, Hagaman, R. Williams, X.-D. Wang, G. Del Cul and J. Fiedor, *J. Phys. Chem. B*, 1998, **102**, 1951–1955.
40 D. Dai, H.-J. Koo, M.-H. Whangbo, C. Soulard, X. Rocquefelte and S. Jobic, *J. Solid State Chem.*, 2003, **173**, 114.
41 A. Groß, *Theoretical Surface Science: A Microscopic Perspective*, Springer-Verlag, Berlin, 2003.
42 C. Doornkamp and V. Ponec, *J. Mol. Catal. A*, 2000, **162**, 19.
43 B. Hammer, K. W. Jacobsen and J. K. Nørskov, *Phys. Rev. Lett.*, 1992, **69**, 1971.
44 G. Mills and H. Jónsson, *Phys. Rev. Lett.*, 1994, **72**, 1124.
45 G. Mills, H. Jónsson and G. K. Schenter, *Surf. Sci.*, 1995, **324**305.
46 T. E. Jackman, J. A. Davies, O. P. Jackson, W. N. Unertl and P. R. Norton, *Surf. Sci.*, 1982, **120**, 389.
47 Q. Ge and D. A. King, *J. Chem. Phys.*, 1999, **111**, 9461.
48 A. Alavi, P. Hu, T. Deutsch, P. L. Silvestrelli and J. Hutter, *Phys. Rev. Lett.*, 1998, **80**, 3650.
49 A. Eichler and J. Hafner, *Phys. Rev. B*, 1999, **59**, 5960.
50 M. Mavrikakis, B. Hammer and J. K. Nørskov, *Phys. Rev. Lett.*, 1998, **81**, 2819–2822.
51 W. X. Li and B. Hammer, *Chem. Phys. Lett.*, 2005, **409**, 1.

